Design and analysis of suspended core channel waveguide made using As_2Se_3 glass system for mid-infrared supercontinuum generation

M. R. Karim[1], Nayem Al Kayed[2],Golap Kanti Dey[3], B. M. A. Rahman[4]

[1]Department of Electrical and Electronic Engineering, Chittagong Independent University, Chittagong, Bangladesh
[2]Department of Electrical and Electronic Engineering, Chittagong University of Engineering and Technology, Chittagong, Bangladesh
[3]Department of Electronics and Telecommunication Engineering, Chittagong Independent University, Chittagong, Bangladesh
[4]Department of Electrical and Electronic Engineering, City University of London, Northampton Square, London, EC1V 0HB, UK

E-mail: mrkarim@ciu.edu.bd

October 2020

Abstract. In this study, we propose a promising 5-mm-long air-clad suspended core channel waveguide made of As_2Se_3 chalcogenide glass for ultrabroadband supercontinuum generation in the mid-infrared. The linear analysis of the proposed waveguide is carried out numerically by considering the potential application of pump source at three different wavelength regions such as 1.55 μm, 2.8 μm, and 3.5 μm. Among several waveguide geometries analyzed, numerical simulation for supercontinuum generation at the output of an optimized structure shows that a flat supercontinuum coverage from 1.5 μm to 15 μm can be predicted using a pump at 3.5 μm with a moderate peak power of 2000 W. To the best of the authors' knowledge, this would be the broadest spectra in the mid-infrared by the suspended planar waveguide design. In addition, waveguide structural imperfection has also been discussed as it is difficult to control the waveguide dimensions during fabrication process precisely. The effect of possible deviations along the transverse dimensions are rigorously analyzed and an imperfection among the several deviations is found which could lead to a substantial supercontinuum bandwidth reduction at the waveguide output. Finally, the degree of coherence of the obtained supercontinuum coverage is also tested and it has been achieved nearly coherent spectral outcome from the proposed suspended waveguide design.

Keywords: Nonlinear optics, Ultrafast optics, Integrated photonics devices, Suspended channel waveguide (SCW), Group-velocity dispersion (GVD), Nonlinearity, Supercontinuum generation (SCG), Chalcogenide glass materials.

1. Introduction

Supercontinuum generation (SCG) has become an interesting field of research in recent years because of having its huge and diverse amount of applications in telecommunication, biomedical-imaging, spectroscopic-measurement, sensing-application, and astronomical observation. At present, researchers are investigating to find a way to generate mid-infrared (MIR) SCG for covering the spectral region 2–20 μm as all atomic molecules in this region offer strong vibrational absorption that is highly promising for spectroscopic applications [1, 2]. Extensive investigations have performed using microstructured fibers for spanning the SCG spectra far into the MIR [3, 4, 5, 6, 7, 8]. Due to technological development in recent years, the on-chip complementary metal-oxide-semiconductor (CMOS) compatible integrated photonic devices have drawn attraction to the researchers for the generation of efficient broadband SCG in the MIR [9]. Ultrabroadband spectral coverage far into the MIR can be obtained by designing planar waveguide employing chalcogenide (ChG) glass systems with the aid of their high Kerr nonlinear properties [10, 11, 12, 13, 14].

Microstructured based fiber design has been used extensively in the last decades for generating SCG in the MIR through controlling the light mode confinement and dispersion variations by varying the various structural parameters of the design [15]. However, in this approach, increasing propagation loss in the case of designing long length micro-structured fibers is standing as a problem [16]. To reduce the propagation loss, the short length, scalable, and low-cost integrated photonic device fabrication is preferred by the researchers nowadays. To address this issue in designing the SCG sources, the planar waveguide is a promising candidate in line with microstructured based fiber design [17, 18, 19, 20]. The prime concern during planar waveguide design is the absorption loss of a bottom layer of the waveguide core in the deep MIR. Suspended type planar waveguide nowadays has emerged as a new kind of integrated photonic device based design that can be utilized for manufacturing optomechanical, nonlinear, and electro-optical devices. The design of this type of waveguide is based on eliminating a bottom layer of a waveguide core by a micro-machining technique which reduces the light absorption in the long-wavelength substantially [21].

In the last decade, the design of broadband SCG sources using the optical planar structure and microstructured based optical fiber have been investigated both the theoretically and experimentally by the several research groups [17, 20, 22, 23, 24, 25, 26, 27, 28, 29, 30, 31, 32, 33, 34, 35]. Table 1 presents a brief summary of MIR SCG coverages obtained by using different types of fibers and waveguides in the recent years. Among the various fiber based work mentioned in this table, Ou *et al.* [24], Petersen *et al.* [25], and Zhao *et al.* [26] experimentally reported MIR spectral coverages of 1.8–14 μm, 2–15.1 μm, and 2–16 μm through step-index fiber made of $Ge_{12}As_{24}Se_{64}$, $Ge_{15}Sb_{25}Se_{60}$, and As_2Se_3 chalcogenide materials, respectively, by applying input power in the MW range. The MIR spectral coverages were also achieved beyond 10 μm using planar rib-waveguides made of $Ge_{11.5}As_{24}Se_{64.5}$ chalcogenide glass system by Yu *et al.* [11, 17]. As planar waveguide suffers substantial absorption loss from the bottom layer of a waveguide core, researchers are nowadays started to design chip-scale suspension type waveguide for the MIR applications [21]. A few research groups until today have investigated the theoretical and the experimental SCG evolution in the MIR using suspended type planar waveguides [36, 37, 38]. Kou *et al.* [36] reports an SCG spanning from 2 to 5 μm in a 12 mm long silicon suspended rib waveguide by pumping with a pulse width of 300-fs at a 4 μm wavelength with an average power of 10 mW. Jing *et al.* [37] numerically investigates broadband SCG using a suspended type As_2Se_3 ridge waveguide by which spectral coverage from 1 to 5.6 μm can be obtained after a 3.1 mm long propagation when pumping wavelength used at a 2.65 μm with a peak power 450 W. Li *et al.* [38] demonstrates numerically the SCG expansion from 1.76 to 14.42 μm in a 0.87 mm long suspended As_2Se_3 ridge waveguide by pumping at 3.3 μm with 100-fs pulse duration and an input power of 900 W.

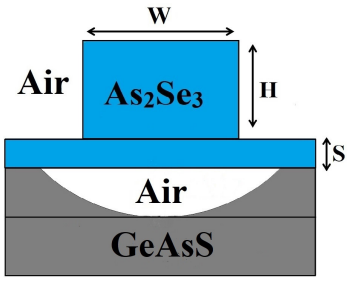

Figure 1. Proposed SCW Geometry

In this numerical work, we have proposed a novel 5 mm long suspended core channel waveguide (SCW) for generating broadband SCG up to the MIR. To see spectral broadening, initially, few SCW geometries are tailored based on width (W), height (H), and suspension thickness (S) variations at 1.55 μm and 2.8 μm wavelengths, respectively. Later one more geometry is optimized by shifting pump wavelength at 3.5 μm considering S = 300 nm. Simulation results at the output of the various SCWs that tailored for pumping at the three different wavelengths

Table 1. Recent results on SCG using various types of fibers and waveguides

Structure type	Core material	Length [mm]	λ_p [μm]	P_p [kW]	T_p [fs]	SC BW [μm]	Study type	Year
SIF	As_2Se_3	85	6.3	7.15×10^3	100	1.4–13.3	Exp.	2014 [1]
SIF	$Ge_{12}As_{24}Se_{64}$	110	4	3	330	1.8–10	Exp.	2015 [28]
SIF	$Ge_{15}Sb_{25}Se_{60}$	200	6	750	150	1.8–14	Exp.	2016 [24]
SIF	As_2Se_3	30	9.8	2.89×10^3	170	2–15.1	Exp.	2016 [23]
SIF	$(Ge_{10}T_{e43})$90-AgI_{10}	140	7	76.7×10^3	150	2–16	Exp.	2017 [26]
PCF	As_2Se_3	50	4.6	10	50	2.6–6.46	Num.	2015 [31]
PCF	As_2Se_3	5	4.1	3.5	50	2–15	Num.	2015 [29]
PCF	$Ge_{10}As_{22}Se_{68}$	40	4	37	250	1–11.5	Exp.	2017 [25]
SCF	As_2Se_3	200	2.5	4.86	200	0.6–4.1	Exp.	2014 [33]
SCF	$As_{38}Se_{62}$	180	4.4	5.2	320	1.7–7.5	Exp.	2015 [34]
SCF	ZBLAN	400	1.56	2.3×10^{-3}	88	0.35–2.4	Num.	2019 [39]
SCF	CCl_4	50	1.55	5	200	0.35–2.3	Num.	2020 [35]
NW	$Ge_{11.5}As_{24}Se_{64.5}$	18	1.55	25	50	1.2–2.5	Num.	2014 [10]
RW	$Ge_{11.5}As_{24}Se_{64.5}$	5	5.3	20×10^3	150	2.5–10	Exp.	2013 [11]
RW	$Ge_{11.5}As_{24}Se_{64.5}$	50	4.184	4.5	330	2–10	Exp.	2016 [17]
RW	As_2Se_3	2.5	2.8	2.5	200	1.2–7.2	Num.	2018 [22]
CW	$Ga_8Sb_{32}S_{60}$	5	2.8	6.5	497	1–9.7	Num.	2017 [18]
CW	$Ge_{22}As_{20}Se_{58}$	8	2.8	24	130	2.5–6.5	Exp.	2018 [19]
SRW	Silicon	12	4	223	300	2–5	Exp.	2018 [36]
SRdW	As_2Se_3	3.1	2.65	0.45	200	1–5.6	Num.	2018 [37]
SRdW	As_2Se_3	0.87	3.3	0.9	100	1.76–14.42	Num.	2019 [38]

Where SIF = step index fiber, PCF = photonic crystal fiber, SCF = suspended core fiber, NW = nanowire, RW = rib waveguide, CW = channel waveguide, SRW = suspended rib waveguide, SRdW = suspended ridge wavegude, Exp. = experimental, Num.= numerical, λ_p = pump wavelength, P_p = pump peak power, T_p = pulse duration, and BW = bandwidth.

show that the SCG can be obtained beyond 15 μm by employing the pump at 3.5 μm wavelength with a peak power of 2000 W. This would be the broadest SCG coverage in the MIR by the planar waveguide design so far. We have also analyzed the effects of unexpected occurrence of imperfections along the transverse dimensions of a waveguide during fabrication. Rigorous analysis considering various possibilities of geometric deviation shows that the occurrence of an even one degree downward angular displacement (horizontal imperfection) could incur substantial SCG bandwidth reduction, which could be more than 20% of the total coverage predicted at the waveguide output. Later in the degree of coherence study, it has been observed nearly coherent SCG output by our proposed design.

2. Modeling and Method

Figure 1 demonstrates the proposed air-clad SCW geometry in which the As_2Se_3 ChG glass system is employed as core and slab/suspension both. Another ChG glass system $Ge_{11.5}As_{24}S_{64.5}$ is used as the substrate during simulation. The required refractive indices of the proposed glass materials used in the simulation are calculated using the Sellmeier equation from [40] over the interesting wavelength range. To characterize an optical waveguide for a certain distribution of the refractive index, the finite-element analysis (FEA) is frequently used as well known computational tool. The FEA based COMSOL Multiphysics is employed to obtain the effective refractive index of a fundamental quasi-transverse electric (FQTE) mode for the proposed SCW geometry. Figure 2 shows the spatial FQTE field (H_y^{11}) profiles, which imply excellent field confinement in the central core region of the proposed SCW structures, at the two different pump wavelengths. This certainly increases the nonlinear interaction which eventually broadens the spectral coverage at the SCW output. The calculated n_{eff} values are utilized to obtain group velocity dispersion (GVD) [41] which is a vital parameter to characterize an optical waveguide for an ultrabroadband SCG generation in the MIR. The waveguide imperfections in the transverse directions are calculated using the following equations:

$$W_{\mathrm{i}} = W \pm 2\Delta W, \tag{1}$$

$$H_{\mathrm{i}} = H \pm \Delta H, \tag{2}$$

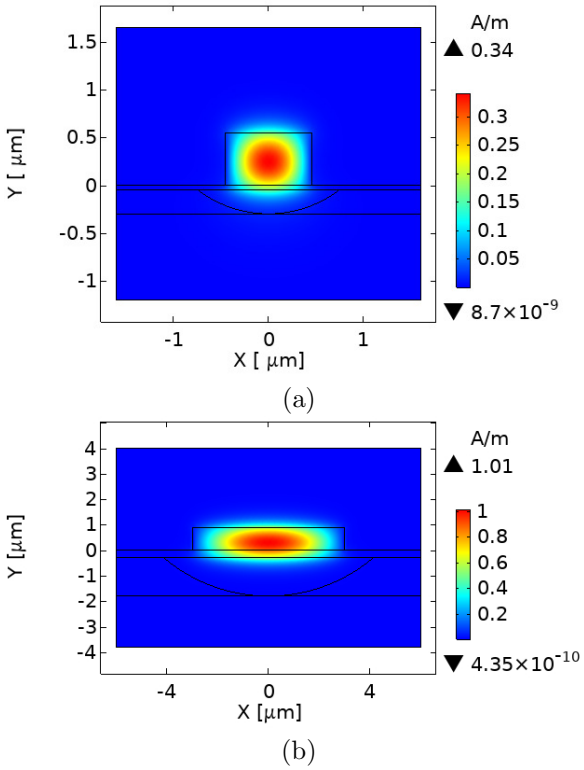

Figure 2. The field profiles of FQTE mode for proposed geometries (uniform cases) (a) at a wavelength of 1.55 μm with structural parameters $W = 900$ nm, $H = 550$ nm, $S = 50$ nm (b) at a wavelength of 3.5 μm with structural parameters $W = 6000$ nm, $H = 900$ nm, $S = 300$ nm.

where W_{i} and H_{i} are expressed as the possible deviated waveguide dimensions after the fabrication process and W and H indicate the waveguide ideal dimensions. Here, $\Delta W = H\ tan\ \theta_{\mathrm{W}}$ and $\Delta H = W\ tan\ \theta_{\mathrm{H}}$, respectively, are the possible amount of deviations along the horizontal and vertical directions where θ_{W} and θ_{H} are the deviation angles along those directions. In Eqs. 1 and 2, +ve deviations indicate outside or upward and -ve deviations imply inside or downward deviations of the proposed waveguide.

To investigate the SCG coverage between the near-IR and the MIR in the waveguide tailored with anomalous GVD characteristics, the light pulse propagation along with its all nonlinear dynamics inside the optimized SCW can be analyzed by numerically solving the well established generalized nonlinear Schrödinger equation (GNLSE) given in Eq. 3. [15].

$$\frac{\partial}{\partial z}A(z,T) = -\frac{\alpha}{2}A + \sum_{k\geq 2}^{12}\frac{i^{k+1}}{k!}\beta_k\frac{\partial^k A}{\partial T^k} + i\gamma\left(1+\frac{i}{\omega_0}\frac{\partial}{\partial T}\right) \times \left(A(z,T)\int_{-\infty}^{\infty}R(T)\mid A(z,T-T')\mid^2 dT'\right), \tag{3}$$

In the Eq. 3, $A(z,T)$ describes the electric field envelop moving with the group velocity $v_g = 1/\beta_1$ ($T = t - \beta_1 z$) where higher order dispersion and angular pump frequency are demonstrated correspondingly by β_k ($k \geq 2$) and ω_0. The parameter α and γ represent the material propagation loss and the nonlinear co-efficient respectively. The response function $R(T)$ is modeled by considering Raman contribution mentioned in Eq. 4 and Eq. 5 [41].

$$R(t) = (1 - f_{\mathrm{R}})\delta(t) + f_{\mathrm{R}}h_{\mathrm{R}}(t), \tag{4}$$

$$h_{\mathrm{R}}(t) = \frac{\tau_1^2 + \tau_2^2}{\tau_1\tau_2^2}\exp\left(-\frac{t}{\tau_2}\right)\sin\left(\frac{t}{\tau_1}\right). \tag{5}$$

The SCG coverages at the output of all the optimized SCWs at different pump wavelengths are investigated by solving the GNLSE [41] using an in-house developed MATLAB software adopting symmetrized split-step Fourier method [42]. The numerical values of Raman responses and assumptions for solving the GNLSE equation are depicted in Table. 2.

Table 2. The Raman parameters of As_2Se_3 materials [42] and the assumptions to solve the GNLSE equation [43] using split-step Fourier method

Parameters	Value considered
f_{R}	0.148
τ_1	23 fs
τ_2	164.5 fs
Fourier grid points	2^{17}
Time step	2.76 fs
Numbers of steps	10^5
Step size	100 nm

3. Numerical Analysis and Result

To obtain a broadband SCG coverage from the near-IR to the far-IR using the optical waveguide proposed, it is not enough to confine the light mode in the core region rather the tailoring of GVD by tuning the waveguide structural parameters. To generate a broadened and efficient SCG spectrum, an optical waveguide must be pumped with a low GVD value, near to the first zero-dispersion wavelength in the anomalous GVD regime [15]. With a low GVD value at the pump wavelength, flat dispersion also plays a key role in the expansion of SCG. On the other hand, another important issue related to the SCG expansion from the near-IR to the far-IR is that the waveguide must be modeled in such a manner that it can be pumped in the longer wavelength region with a commercially available pump source.

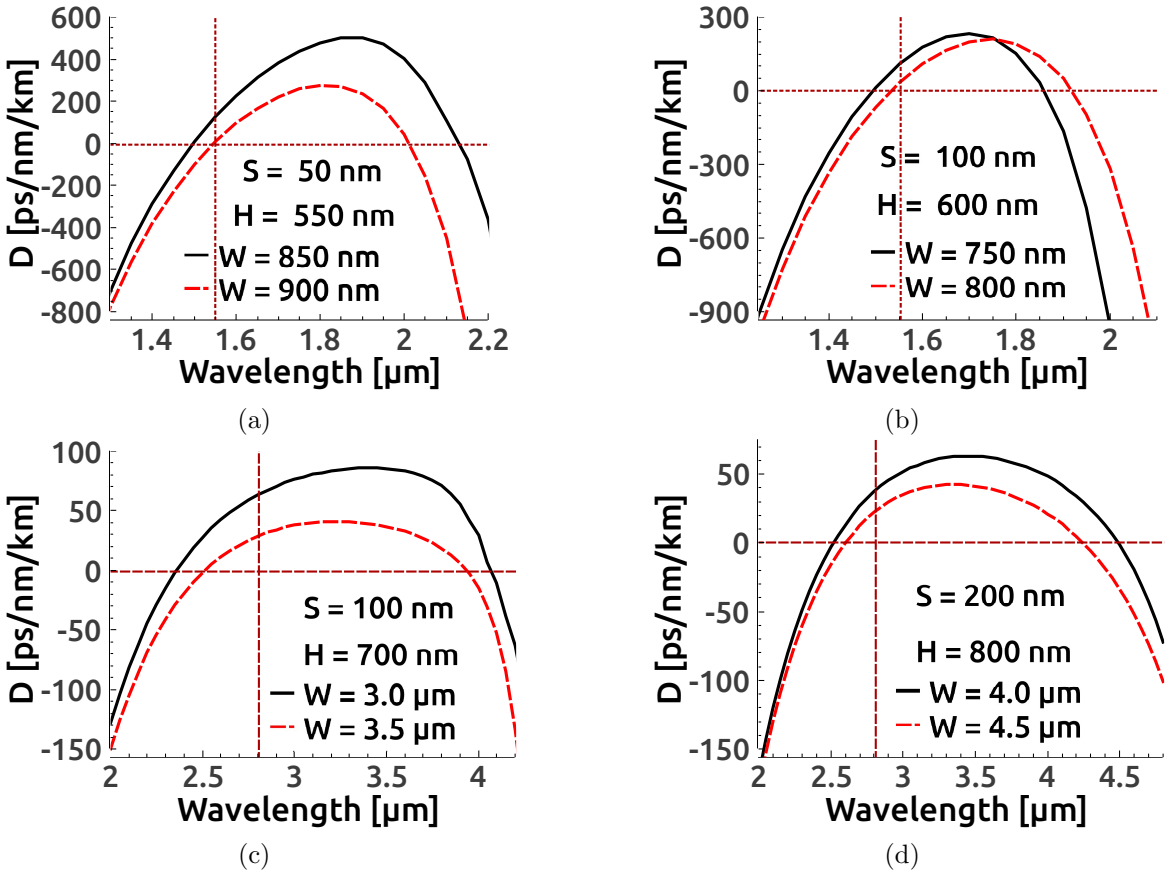

Figure 3. The GVD curves are tailored based on H and W of the proposed SCW for the potential application of pump at 1.55 μm considering (a) $S = 50$ nm; (b) $S = 100$ nm. The SCW is further optimized by varying its dimensions for pumping at 2.8 μm keeping (c) $S = 100$ nm; (d) $S = 200$ nm.

To fulfill this requirement and to see such an ultra-broadband SCG expansion, our proposed waveguide structures are tailored for pumping at three different positions from low to higher wavelengths such as 1.55 μm, 2.8 μm, and 3.5 μm, respectively. Initially, to observe the spectral broadening at the output of the proposed SCWs that are tailored for pumping at 1.55 μm wavelength, a TE polarized 50-fs full-width at half-maximum (FWHM) sech pulse with an input peak power of 100 W is applied. On the other hand, to observe the spectral coverage further into the MIR, a few more SCW structures are tuned for pumping at 2.8 μm and 3.5 μm with a sech pulse of 100-fs duration [44] and an input peak power 1000 W and 2000 W, respectively.

As the support of a core/channel of a suspended type waveguide depends on slab thickness, S, a number of SCW geometries are tailored for the broadband SCG analysis by assuming different suspension thickness, S as well as by assuming different pump wavelength proposed. Considering pump wavelength at 1.55 μm and fixing S at 50 nm, following the GVD tuning criteria described above, initially, two waveguides are optimized by taking W: 850-900 nm and keeping H constant at 550 nm. Enhancing S to 100 nm, two more structures are tuned by considering W: 750-800 nm keeping H at 600 nm at the same pump wavelength. The GVD values, mode effective areas and nonlinear parameters for the above two sets of SCWs are calculated as D: 126–6 ps/nm/km, 108–33 ps/nm/km, A_{eff}: 0.42–0.44 μm^2, 0.42–0.44 μm^2 and γ: 106–102 /W/m, 106–102 /W/m, respectively. Figures 3(a) and 3(b) depict the tailored GVD curves for the four different SCW structural variations proposed above. The corresponding numerical simulations for the SCG coverage are illustrated in Figs. 4(a) and 4(b), respectively. Maximum SCG coverage obtained from the SCWs that tailored for pumping at 1.55 μm in the range 1.2–2.3 μm with an input peak power of 100 W. To see the further spectral broadening, next four structural variations are tailored to pump them at 2.8 μm considering two different S at 100 nm or 200 nm whose GVD curves are depicted in Figs. 3(c) and 3(d), respectively. The GVD values, mode effective areas and nonlinear parameters for those variations are computed as D: 63–29 ps/nm/km,

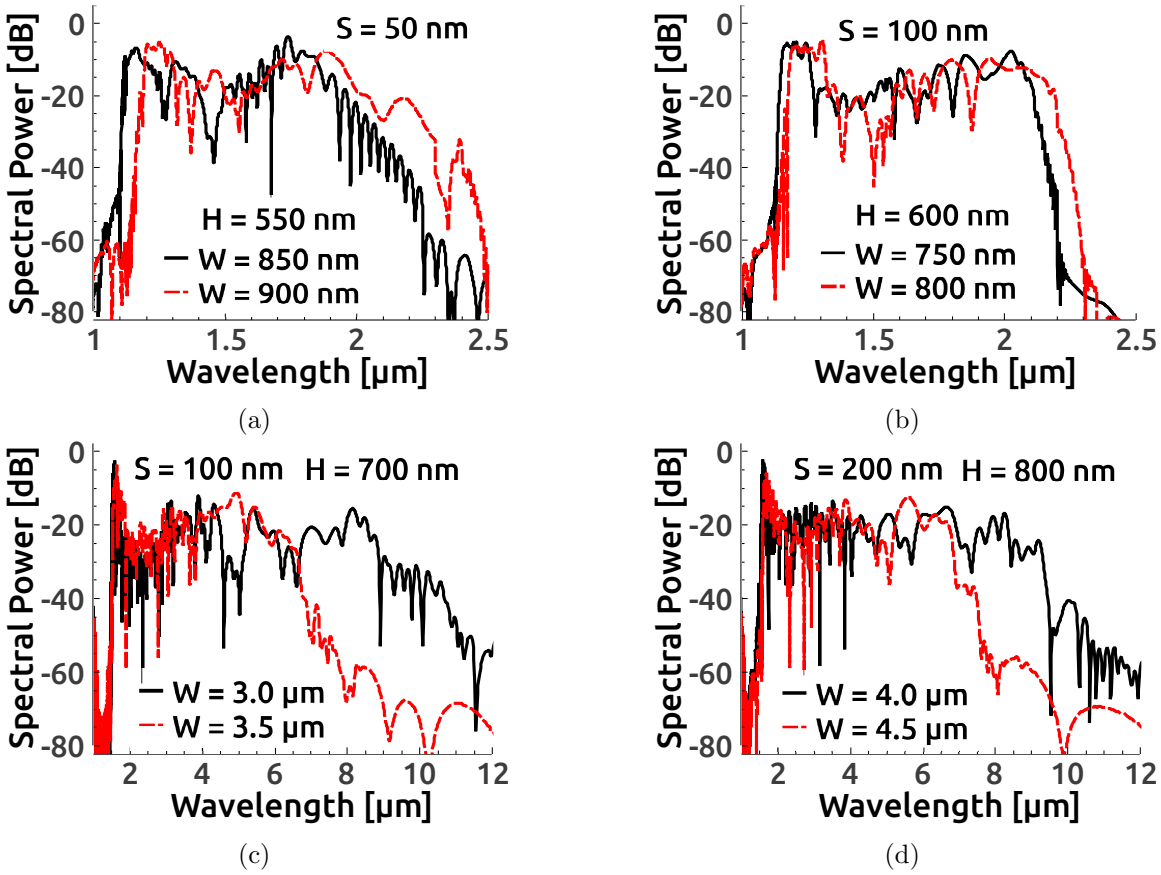

Figure 4. The SCG coverages predicted from the output of the optimized SCW at two different wavelengths (1.55 μm and 2.8 μm, respectively) after simulations corresponding to the four GVD sets depicted in Fig. 2. The input peak power are used as 100 W and 1000 W for top and bottom rows, respectively.

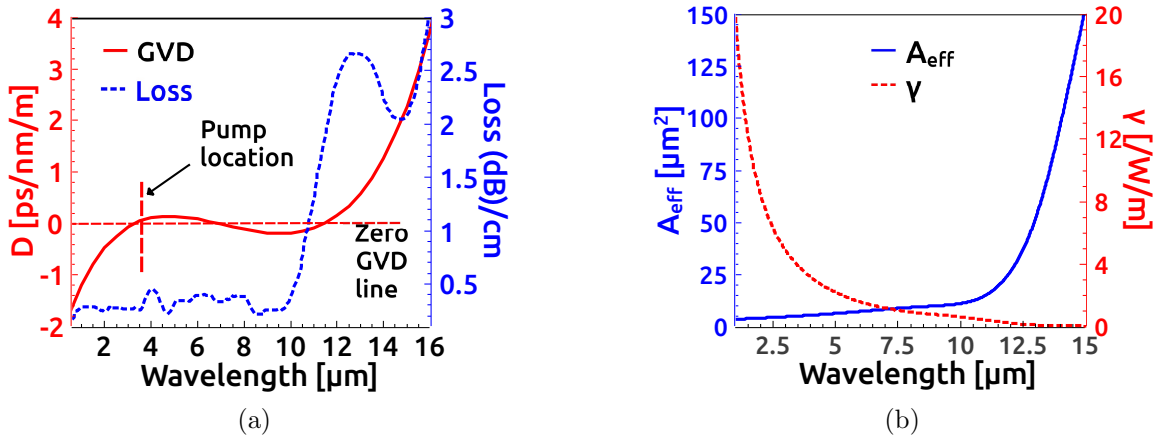

Figure 5. The SCW geometry (W = 6 μm, H = 0.9 μm, S = 300 nm) optimized to see further SCG expansion into the MIR after the pump shifted at 3.5 μm: (a) GVD curve and material loss; and (b) Wavelength dependent mode effective areas and their corresponding nonlinear co-efficients up to the desired wavelengths.

37–22 ps/nm/km, A_{eff}: 1.93–2.2 μm^2, 2.79–3.08 μm^2 and γ: 13–11 /W/m, 9–8 /W/m, respectively. After the SCG simulations, their corresponding results are plotted in Figs. 4(c) and 4(d), respectively. The highest spectral coverage up to 10 μm can be achieved with a peak power of 1000 W by these designs. Finally, one more SCW geometry is tailored to see deep MIR coverage by shifting the pump at 3.5 μm considering S at 300 nm. The GVD curve for this design is shown in Fig. 5(a). Interestingly it can be seen from Fig. 5(a) that flat dispersion with low GVD values up to the long-wavelength has been observed which is highly

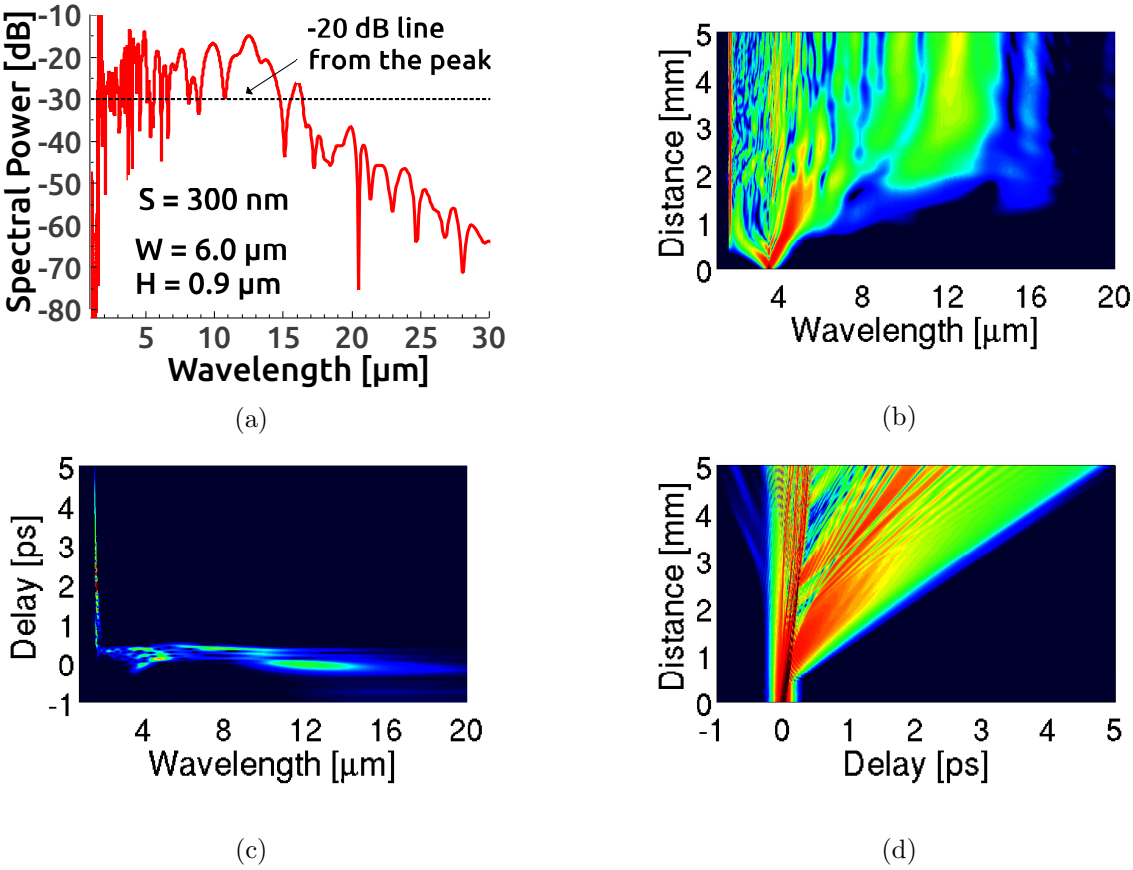

Figure 6. The MIR SCG expansion for the optimized SCW geometry (W = 6 μm, H = 0.9 μm, S = 300 nm) by shifting pump at 3.5 μm: (a) Spectral coverage; (c) Spectral density plot; (c) Spectrogram; and (d) Temporal density plot. The input peak power is used 2000 W for this design.

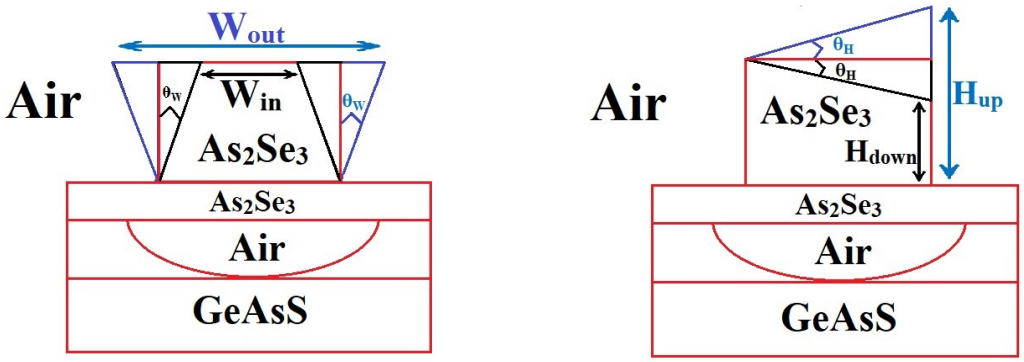

Figure 7. Possible unexpected angular deviations during the SCW fabrication in the (a) vertical directions; and (b) horizontal directions.

suitable for an ultra-broadband SCG expansion from the near-IR to the far-IR regime. The wavelength-dependent material propagation loss is considered as loss edge given in Fig. 5(a) [45] at the input of each SCW during the numerical simulation. Figure 5(b) shows the wavelength dependent A_{eff} plot and its corresponding γ plot up to the desired wavelength. The value of D, A_{eff} and γ at the pump wavelength are computed as 49 ps/nm/km, 5.03 μm^2 and 3.93 /W/m, respectively. Simulation results for this design from Figs. 6(a) to 6(c) show that the spectral coverage in the range 1.5–15 μm can be predicted with a moderate peak power of 2000 W. Thus, owing to a low and flat GVD curve, it is possible to obtain flat SCG expansion up to 15 μm from our proposed design. The final waveguide structure proposed in this work is optimized

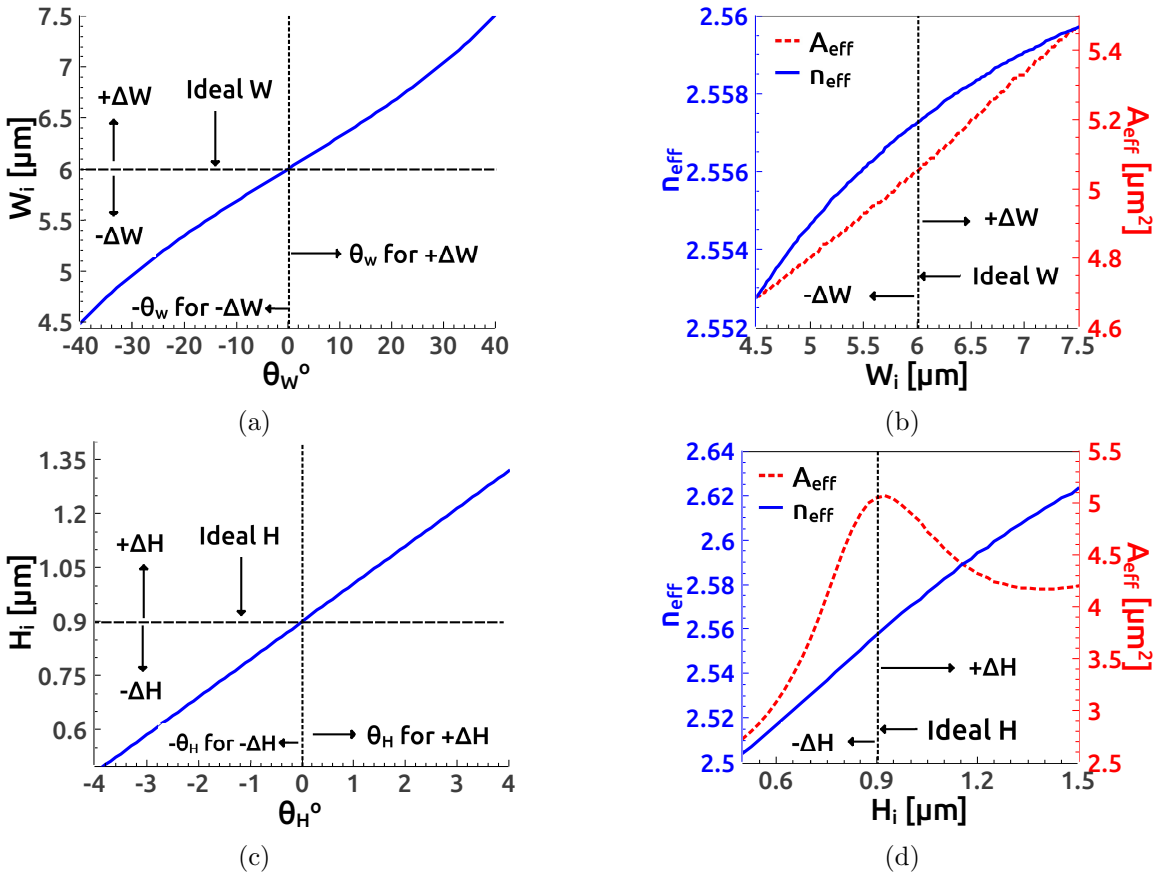

Figure 8. Imperfections/perturbations ($W_\mathrm{i}, H_\mathrm{i}$) calculated along the waveguide transverse directions: (a) through the variation of θ_W; (b) and the effect of ΔW on n_eff and A_eff; (c) through the variation of θ_H; and (d) the effect of ΔH on n_eff and A_eff considering the ideal structure of $W = 6$ μm, $H = 0.9$ μm, $S = 300$ nm and a pump wavelength of 3.5 μm.

for obtaining the highest spectral flatness from the several waveguide geometries analyzed. In case of our proposed design, the spectral flatness of the final SCG coverage is predicted through observation of Fig. 6(a) and the flatness is assumed here considering ±10 dB spectral components fluctuation from its mean value over the entire SCG bandwidth predicted.

As seen from temporal density plot of Fig. 6(d), soliton fission occurs around 1 mm for the soliton order of 9. After fission, multiple fundamental solitons are induced due to the inclusion of higher-order dispersion terms, and here up to 12$^{\mathrm{th}}$ number of higher-order terms are added while conducting the numerical simulations. The spectra, produced by the fundamental solitons induced after fission, shifts towards the longer wavelength (red-shifted) due to the intrapulse Raman scattering which produces numerous peaks in the spectrum. At the same time, the phase-matched dispersive wave (blue shifted) is generated, which lies in the short wavelength side of the spectrum. While shifting to the long-wavelength pumping during simulation, the waveguide input peak power was increased from 100 W to 1000 W, and eventually, it became 2000 W at a pump wavelength of 3.5 μm. The input power of the proposed waveguide is increased while the pump source shifting to a longer wavelength as the nonlinear value decreases with the pump wavelength shifting. If we look into the nonlinear values of the waveguide optimized for pumping at three different wavelengths proposed, we can see the value of a nonlinear parameter fall down approximately 10 times at 2.8 ($\approx$ 8$\sim$12 /W/m) than 1.55 μm ($\approx$ 102$\sim$106 /W/m) and later it becomes less than half at 3.5 μm ($\approx$ 4 /W/m) compared to the 2.8 μm wavelength. Corresponds to the reduction of the nonlinear parameter with a pump wavelength, the pump powers are enhanced accordingly during the numerical simulations. In this work, however, $\mathrm{A_{eff}}$ dependent γ is used up to the wavelength range of interest during all the numerical simulations of SGC generation. During the values of γ calculation, the Kerr nonlinear refractive index, n_2 is considered as 1.1 $\times$ 10^{17} m^2/W [23].

During the fabrication of an optical waveguide, unexpected structural imperfection/deviation can happen either in the horizontal direction or in the vertical

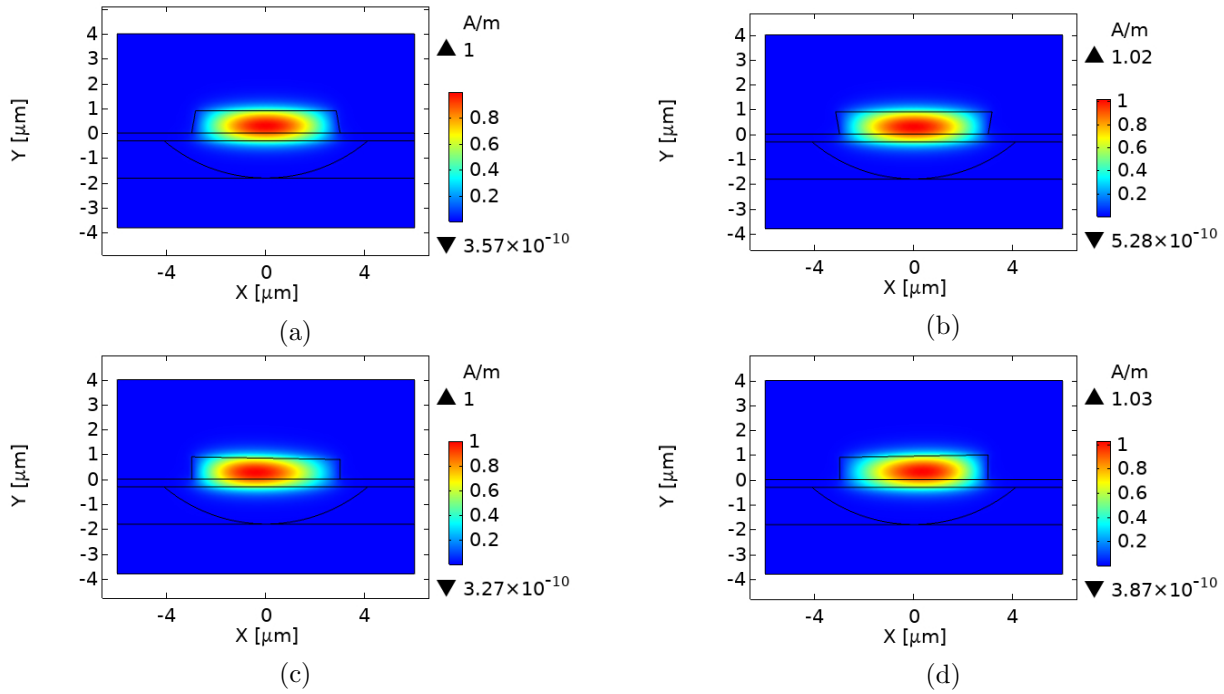

Figure 9. The field profiles of FQTE modes (H_y^{11}) for (a) $\theta_W = 10$ degree inside (from both directions); (b) $\theta_W = 10$ degree outside (from both directions); (c) $\theta_H = 1$ degree down; (d) $\theta_H = 1$ degree up for the perturbed waveguide geometry, $W = 6$ μm, $H = 0.9$ μm, $S = 300$ nm at a wavelength of 3.5 μm.

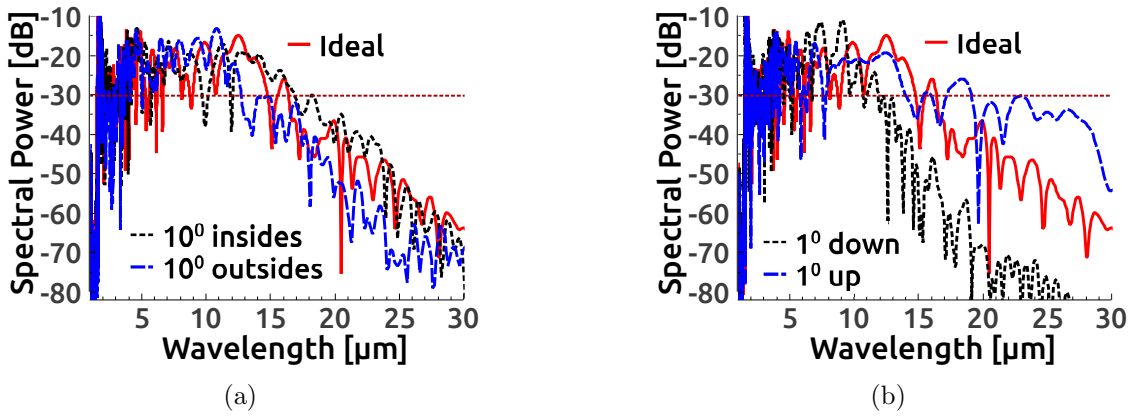

Figure 10. Spectral outcome comparisons between ideal case and perturbed waveguide for possible angular displacements/deviations (a) in vertical directions; (b) in horizontal directions.

direction. Vertical imperfection can occur on either side or in both sides inward or outward directions simultaneously with a displacement angle, $\theta_{\rm W}$ as shown in Fig. 7(a). Horizontal imperfection can happen either upward or downward direction with an angle, $\theta_{\rm H}$ as shown in Fig. 7(b). Depending on the occurrence of the direction of angular displacement, waveguide's $W_{\rm i}$ or $H_{\rm i}$ changes according to the Eq. 1 or Eq. 2, respectively. Figure 8(a) shows $W_{\rm i}$ changes with the $\theta_{\rm W}$ variations either of inside or outside deviations. For vertically perturbed waveguide with a maximum of 10 degree angular displacement in both the inward or the outward directions as shown in Fig. 8(a), the $W_{\rm i}$ of waveguide changes to $W_{\rm in} = 5.677$ μm or $W_{\rm out} = 6.317$ μm, respectively. The GVD value obtained for the inward or the outward deviation is 50.75 ps/nm/km or 47.37 ps/nm/km, respectively, which is approximately the same as the D value of a ideal waveguide. From Fig. 8(b), the $A_{\rm eff}$ is obtained for both the cases nearly the same value as 5.12 μm^2 which is approximately equal to the $A_{\rm eff}$ obtained by the ideal waveguide. This yields approximately equal γ value which is 3.9 /W/m for the SCW either of ideal or imperfection. On the other hand, in the case of horizontal imperfection, for $\theta_{\rm H} = 1$ degree upward or downward angular displacement as can be seen from Fig. 8(c), the waveguide $H_{\rm i}$

changes either to $H_{\rm up}$ = 1.005 μm or $H_{\rm down}$ = 0.795 μm which results waveguide GVD value either D = 53 ps/nm/km or 45 ps/nm/km, respectively. Unlike the vertical deviation, the GVD value changes in this case up to 4 ps/nm/km even in a 1-degree horizontal imperfection. The $A_{\rm eff}$ obtained for either case of the deviated waveguide as illustrated in Fig. 8(d) is 4.87 μm^2 or 4.49 μm^2 which yields the γ value to either 4.1 /W/m or 4.4 /W/m, respectively. In case of horizontal deviations, an interesting phenomenon, unlike vertical deviation, is observed for the upward angular displacement ($+\theta_{\rm H}$) or the resulting positive deviation ($+\Delta H$) of the waveguide. It is clearly seen from the red-dotted curve of Fig. 8(d) that the $A_{\rm eff}$ of the deviated waveguide decreases after ideal H = 0.9 μm with increasing $H_{\rm i}$ which is observed in reverse manner in the case of vertically perturbed waveguide where $A_{\rm eff}$ variations are shown by the red-dotted line in Fig. 8(b). The mode profiles, FQTEs of all possible imperfections assumed for the proposed SCW are shown in Fig. 9.

The simulation result of SCG for either case of vertically deviated waveguide along with the spectral coverage of a ideal waveguide is shown in Fig. 10(a). This result is obtained by the same power and pulse width used as before. No significant variation is observed in the case of the vertically perturbed waveguide for the maximum angular deviation of 10 degrees either of both the inward or both the outward imperfections. On the other hand, the spectral coverage of horizontal deviations with the same power and the pulse width are depicted in Fig. 10(b). In the case of a 1-degree horizontal downward deviation, it is apparent from Fig. 10(b) that the SCG expansion gets narrowing at 12 μm which is nearly 3 μm less (approximately 20% reduction) than that of the spectra obtained by the ideal waveguide. Thus, among many possible variation of imperfections found, the horizontally downward angular deviation shows highly sensitive to the desired SCG coverage achievement at the waveguide output. Even less than a 1 degree horizontally downward perturbation could lead to a 20% bandwidth reduction at the SCW output.

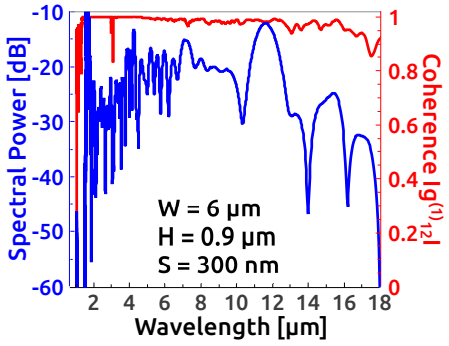

Figure 11. Degree of coherence, $|g^{(1)}_{12}|$ for the output spectral coverage of the SCW structure, W = 6 μm, H= 0.9 μm, and S =300 nm.

Finally, the degree of coherence of the spectral outcome from our proposed waveguide is tested. During coherence study, the first degree of coherence, $|g^{(1)}_{12}|$ [46] is used to characterize the SCG output shown in Fig. 6(a). To calculate $|g^{(1)}_{12}|$, the ensemble average of thirty number of different independent SCG spectrum pairs with different quantum noise seeds are generated. The calculated values of $|g^{(1)}_{12}|$ are then plotted concerning the desired wavelengths, which shown in Fig 11. From the coherence study, it is found that the spectral coverage obtained from our proposed waveguide is nearly coherent ($|g^{(1)}_{12}| \approx 1$) which only becomes possible owing to low input power with fs pulse and can be a potential candidate for the applications such as spectroscopy and optical coherence tomography.

4. Conclusion

In this study, a promising ultrabroadband 5 mm long suspended channel waveguide SCG source has been proposed, which is designed using As_2Se_3 glass system as a core and air as upper and lower claddings. To see the spectral coverage from near-IR to far-IR, three categories of waveguide geometry are tailored for pumping them in either of the three different wavelengths proposed. Simulation result at the output of the last category waveguide model, which is tailored for pumping at 3.5 μm, shows that the flat SCG coverage can be predicted in the range 1.5-15 μm with a moderate peak power of 2000 W, which would, as per as the authors' knowledge, be the widest spectral range obtained by any planar waveguide design in the MIR. Moreover, the vital factor such as the effects of possible waveguide imperfection on spectral coverage, considering various angular deviations along the waveguide transverse dimensions, are discussed. Among various imperfections analyzed after fabrication process, the horizontal imperfection is found to be more sensitive, which caused significant spectral coverage reduction at the output of our proposed SCW design. Another vital concern is coupling loss between the proposed waveguide and the pump source, which needs to be taken into account while conducting experimental work. Various losses including loss due to mode-area mismatch between pump and waveguide, Fresnel reflection loss at the coupling point or from index matching liquid from interfaces might result in coupling efficiency below 20% [36] at the waveguide input. Therefore, to achieve similar SCG coverage experimentally by our proposed design, more input power will be required than the pump power assumed in this work. We finally tested

the first degree of coherence of the SCG outcome and achieved a nearly coherent spectral outcome from our proposed design. The main advantage of the suspended type waveguide design is that by using this design lower cladding absorption loss may substantially be reduced in the longer wavelength region which may not possible for a traditional planar waveguide design. This numerical work may encourage the researchers to lead to a fresh experimental activity in the design of a suspended planar waveguide for the MIR SCG generation and it could be used in a variety of the MIR region applications such as sensing, spectroscopic application, biological imaging and many more.

Data Availability Statement

The data that support the findings of this study are available from the corresponding author upon reasonable request.

References

[1] Petersen C R, Møller U, Kubat I, Zhou B, Dupont S, Ramsay J, Benson T, Sujecki S, Abdel-Moneim N, Tang Z *et al.* 2014 *Nature Photonics* **8** 830

[2] Schliesser A, Picqué N and Hänsch T W 2012 *Nature Photonics* **6** 440

[3] Dudley J M and Taylor J R 2009 *Nature Photonics* **3** 85

[4] Tajima K, Zhou J, Nakajima K and Sato K 2004 *Journal of Lightwave Technology* **22** 7

[5] Knight J and Russell P S J 2002 *Science* **296** 276–277

[6] Knight J, Birks T, Russell P S J and Atkin D 1996 *Optics Letters* **21** 1547–1549

[7] Cregan R, Mangan B, Knight J, Birks T, Russell P S J, Roberts P and Allan D 1999 *Science* **285** 1537–1539

[8] Ma P, Choi D Y, Yu Y, Gai X, Yang Z, Debbarma S, Madden S and Luther-Davies B 2013 *Optics Express* **21** 29927–29937

[9] Oh D Y, Sell D, Lee H, Yang K Y, Diddams S A and Vahala K J 2014 *Optics Letters* **39** 1046–1048

[10] Karim M R, Rahman B M A and Agrawal G P 2014 *Optics Express* **22** 31029–31040

[11] Yu Y, Gai X, Wang T, Ma P, Wang R, Yang Z, Choi D Y, Madden S and Luther-Davies B 2013 *Optical Materials Express* **3** 1075–1086

[12] Gai X, Han T, Prasad A, Madden S, Choi D Y, Wang R, Bulla D and Luther-Davies B 2010 *Optics Express* **18** 26635–26646

[13] Lamont M R, Luther-Davies B, Choi D Y, Madden S and Eggleton B J 2008 *Optics Express* **16** 14938–14944

[14] Yeom D I, Mägi E C, Lamont M R E, Roelens M A F, Fu L and Eggleton B J 2008 *Optics Letters* **33** 660–662

[15] Dudley J M, Genty G and Coen S 2006 *Reviews of Modern Physics* **78** 1135

[16] Corwin K L, Newbury N R, Dudley J M, Coen S, Diddams S A, Weber K and Windeler R 2003 *Physical Review Letters* **90** 113904

[17] Yu Y, Gai X, Ma P, Vu K, Yang Z, Wang R, Choi D Y, Madden S and Luther-Davies B 2016 *Optics Letters* **41** 958–961

[18] Saini T S, Tiwari U K and Sinha R K 2017 *Journal of Applied Physics* **122** 053104

[19] Morris J M, Mackenzie M D, Petersen C R, Demetriou G, Kar A K, Bang O and Bookey H T 2018 *Optical Materials Express* **8** 1001–1011

[20] Karim M R, Ahmad H, Ghosh S and Rahman B M A 2018 *Journal of Applied Physics* **123** 213101

[21] Stievater T H, Pruessner M W, Rabinovich W S, Park D, Mahon R, Kozak D A, Boos J B, Holmstrom S A and Khurgin J B 2015 *Applied Optics* **54** F164–F173

[22] Saini T S, Hoa N P T, Nagasaka K, Luo X, Tuan T H, Suzuki T and Ohishi Y 2018 *Applied Optics* **57** 1689–1693

[23] Cheng T, Nagasaka K, Tuan T H, Xue X, Matsumoto M, Tezuka H, Suzuki T and Ohishi Y 2016 *Optics Letters* **41** 2117–2120

[24] Ou H, Dai S, Zhang P, Liu Z, Wang X, Chen F, Xu H, Luo B, Huang Y and Wang R 2016 *Optics Letters* **41** 3201–3204

[25] Petersen C R, Engelsholm R D, Markos C, Brilland L, Caillaud C, Trolès J and Bang O 2017 *Optics Express* **25** 15336–15348

[26] Zhao Z, Wu B, Wang X, Pan Z, Liu Z, Zhang P, Shen X, Nie Q, Dai S and Wang R 2017 *Laser & Photonics Reviews* **11** 1700005

[27] Hudson D D, Antipov S, Li L, Alamgir I, Hu T, El Amraoui M, Messaddeq Y, Rochette M, Jackson S D and Fuerbach A 2017 *Optica* **4** 1163–1166

[28] Yu Y, Zhang B, Gai X, Zhai C, Qi S, Guo W, Yang Z, Wang R, Choi D Y, Madden S *et al.* 2015 *Optics Letters* **40** 1081–1084

[29] Saini T S, Kumar A and Sinha R K 2015 *Journal of Lightwave Technology* **33** 3914–3920

[30] Markos C, Travers J C, Abdolvand A, Eggleton B J and Bang O 2017 *Reviews of Modern Physics* **89** 045003

[31] Saghaei H, Ebnali-Heidari M and Moravvej-Farshi M K 2015 *Applied Optics* **54** 2072–2079

[32] Habib M S, Markos C, Bang O and Bache M 2017 *Optics Letters* **42** 2232–2235

[33] Mouawad O, Picot-Clémente J, Amrani F, Strutynski C, Fatome J, Kibler B, Désévédavy F, Gadret G, Jules J C, Deng D *et al.* 2014 *Optics letters* **39** 2684–2687

[34] Møller U, Yu Y, Kubat I, Petersen C R, Gai X, Brilland L, Méchin D, Caillaud C, Troles J, Luther-Davies B *et al.* 2015 *Optics Express* **23** 3282–3291

[35] Sharafali A and Nithyanandan K 2020 *Applied Physics B* **126** 1–12

[36] Kou R, Hatakeyama T, Horng J, Kang J H, Wang Y, Zhang X and Wang F 2018 *Optics Letters* **43** 1387–1390

[37] Jing S, Mei C, Wang K, Yuan J, Yan B, Sang X and Yu C 2018 *Optics Communications* **428** 227–232

[38] Li Z, Yuan J, Mei C, Li F, Zhou X, Yan B, Wu Q, Wang K, Sang X, Long K *et al.* 2019 *Applied Optics* **58** 8404–8410

[39] Li Y, Wang L, Liao M, Zhang L, Bi W, Xue T, Liu Y, Zhang R and Ohishi Y 2019 *Optical Materials Express* **96** 109281

[40] Ung B and Skorobogatiy M *Optics Express* **18** 8647–8659

[41] Agrawal G P 2013 *Nonlinear fiber optics, 5th ed.* (Academic Press)

[42] Karim M R, Ahmad H, Ghosh S and Rahman B M A 2018 *Optical Fiber Technology* **45** 255–266

[43] Ahmad H, Karim M R and Rahman B M A 2019 *Laser Physics* **29** 025301

[44] Tang Y, Wright L G, Charan K, Wang T, Xu C and Wise F W 2016 *Optica* **3** 948–951

[45] Mo K, Zhai B, Jianfeng L, Coscelli E, Poli F, Cucinotta A, Selleri S, Wei C and Liu Y 2017 *Chinese Physics B* **26** 054216

[46] Gu X, Kimmel M, Shreenath A P, Trebino R, Dudley J M, Coen S and Windeler R S 2003 *Optics Express* **11** 2697–2703